Scanning electron microscopy imaging of ultra-high aspect ratio hole features

Aron J. Cepler[a,b], Benjamin Bunday[a], Bradley L. Thiel[a,b], John S. Villarrubia[c]

[a]SEMATECH, NY, 12203, USA; [b]College of Nanoscale Science and Engineering, State University of NY at Albany, Albany NY 12203, USA; [c]Semiconductor and Dimensional Metrology Division, National Institute of Standards and Technology, Gaithersburg, MD, 20899, USA [1].

ABSTRACT

In-line, non-destructive process control metrology of high aspect ratio (HAR) holes and trenches has long been a known gap in metrology. Imaging the bottoms of at-node size contact holes in oxide with aspect rations beyond 10:1 has not yet been demonstrated. Nevertheless, holes and trenches of 30:1, 40:1, or even 60:1 will soon enter production, with these etches being applied to various homogeneous and multi-layer stacks of Si and SiO_2. The need comes from Moore's Law and increasing functional density on microchips, on which true 3D memory devices will soon be manufactured. These can take many different forms, but a common building block will be these ultra-HAR etched features. In this work, we show experimental results and simulations from the NIST JMONSEL program to assess the feasibility of measuring such features using both conventional low voltage scanning electron microscopy (SEM) and higher beam energies and low vacuum conditions to ameliorate charging. In our measurements, higher voltage SEM did not improve upon conventional critical dimension (CD)-SEM. Simulations suggest the reason is a failure to overcome a negative oxide potential. Although a signal can in principle be detected from the bottom of contact holes in typical imaging conditions in the CD-SEM, it is likely that it will be very small and possibly below the noise floor.

Keywords: CD-Metrology, 3D Memory, CD-SEM, contact holes, HAR features

1. INTRODUCTION

The inspection of high aspect ratio (HAR) features is an important goal in high volume manufacturing (HVM) metrology. Many different applications, including logic contacts, shallow trench isolations (STIs), and 3D memory features, require inspection to monitor the lithographic processes in creating HAR structures. Monitoring of the top and bottom critical dimension (CD), the hole profiles, and the sidewall roughness is critical [[1]-[3]]. Additionally, any residues on the sides or the bottoms of the hole must be identified. The goal of this work is to evaluate different techniques that may be able to accurately image the bottoms of HAR features, which include trenches and contact holes.

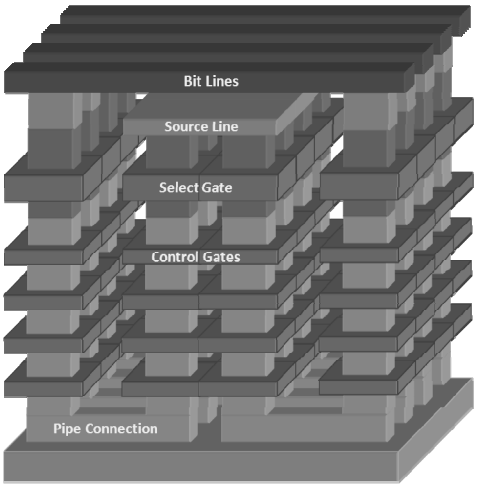

Figure 1: Diagram of pipe-shaped bit cost scalable (P-BiCS) flash memory cell, which consists of pipe-shaped NAND strings folded in a U shape [1]. This is an example of the types of 3D memory devices that will require HVM metrology.

For memory devices to continue to progress by Moore's Law, memory integrated circuit manufacturers are migrating beyond conventional planar designs to build multiple levels of gates into 3D structures. These vertical architectures lead to new challenges in semiconductor processing technology [1]. As shown in Figure 1, the basic building

[1] Contributions by the National Institute of Standards and Technology are not subject to copyright in the United States.

Metrology, Inspection, and Process Control for Microlithography XXVI, edited by Alexander Starikov,
Proc. of SPIE Vol. 8324, 83241N · © 2012 SPIE · CCC code: 0277-786X/12/$18 · doi: 10.1117/12.916552

blocks of these features are deep HAR trenches and holes in oxide, silicon, or multiple alternating layers of oxide and silicon.

3D memory structures present many metrology challenges due to their HAR characteristics. HAR contact holes and trenches at half-pitch dimensions are known gaps in CD and profile metrology in the International Technology Roadmap for Semiconductors (ITRS) [2]. The same kinds of measurement limitations have, to some extent, already been apparent with etched contact holes and shallow trench isolation (STI) trenches in logic for recent ITRS nodes. Furthermore, the problem is increasing with shrinking dimensions. HAR etching is difficult, with 30:1, 40:1, or even 60:1 ARs necessary to form a vertical circuit path among stacked gates. Process control of the bottom of the CD, profile, and detection of polymeric etch residues is required for HVM. While through-silicon vias may have a similar or higher aspect ratio, they are comparatively huge; 3D memory device features will include hole and trench structures with bottom CD sizes at ITRS node dimensions [2], from 0.5 μm to 2 μm deep. This introduces an entirely new set of gaps in metrology capability as the quest for non-destructive measurements of such features has yet to achieve the necessary sensitivity and resolution. Moreover, the physics of these measurements is incompatible with the extremely deep and geometrically confined volumes involved. Charged particle imaging techniques such as CD-SEM and helium ion microscopy [4] have sensitivity limitations arising from sidewall charging, as only a small fraction of scattered particles follow escape trajectories that reach the detector. Also, many optical techniques, especially those that operate off-axis near the critical angle, suffer from a very small fraction of the interrogating light reaching the feature bottom and reflecting upwards to the detector. Thus, in most cases, the various metrology techniques in their present forms will suffer low signal-to-noise ratios (SNRs) on such features.

Many technologies are being explored at SEMATECH to enable HVM of HAR features [5], including both SEM-based imaging techniques as discussed in this paper and spectroscopic techniques such as scatterometry, critical dimension small angle X-ray spectroscopy (CD-SAXS) [6], model-based infrared reflectometry (MBIR) and others. Results are still forthcoming, but CD-SAXS and scatterometry at normal incidence, MBIR, and HV-SEM may have some capability in this application space. CD-SAXS is currently a lab technique, but X-ray sources with higher brightness offer possibilities for transforming this technique into a feasible HVM metrology tool. MBIR takes advantage of the transparency of the various applicable materials to infrared and thus may have sensitivity to some feature aspects. Normal incidence scatterometry may be feasible as more incident light can reach the bottom for potentially improved SNR. HV-SEM is being considered for potentially providing the capability to charge HAR holes in such a way that reflected incident or secondary electrons can more easily escape the bottom of the feature [5].

To examine this problem, SEMATECH fabricated a sample set containing a series of arrays of contact holes. Each array is approximately 150 μm by 150 μm. The arrays are named according to the convention CwxPyz, where Cwx refers to the top diameter wx of the holes in the array and Pyz refers to the pitch yz of the holes (distances measured in nanometers). The narrowest holes in the sample are in the C60P120 array, while the widest holes are in the C100P200 array. One sample set contains 500 nm deep holes; the other contains 1100 nm deep holes. The holes are etched through

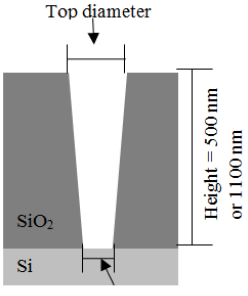

Figure 3: Schematic of the sample structure

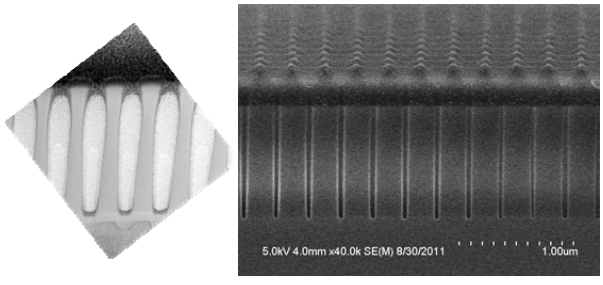

Figure 2: SEM images of focused ion-beam (FIB) cross sectioned samples used in this work.
Left: 500 nm deep holes with 35 nm bottom CD.
Right: 1100 nm deep holes with 30 nm bottom CD.
The profiles are basically trapezoidal with the top larger than the bottom. The apparent closing at the top of the holes on the left is an artifact of the misalignment of the FIB cut.

a SiO_2 layer and terminate at a silicon layer. A schematic of the holes is shown in Figure 2, and cross-sectional images of these samples are shown in Figure 3.

Imaging HAR features is a non-trivial exercise, as there are a number of physical processes which occur during imaging.

For conventional CD-SEM imaging (operating with a beam energy of approximately 500 eV to 800 eV), primary beam electrons tend to come to rest at a depth of some tens of nanometers, depending upon the landing energy. Along the paths of the primary electrons, secondary electrons (SEs) generated within a few nanometers of the surface can escape and leave a net positive charge on the surface. SEs generated at depths greater than a few nanometers generally cannot escape the sample. The upper surface of the oxide therefore charges positively with a negative layer some distance below. The positive layer produces a field that helps extract negative SEs from the bottom of the contact hole. The layer of negative charge will partially counteract the positive charge on the surface and make it more difficult for the SEs from the hole bottom to escape. However, because the initial total yield is greater than one in this energy range, the net charge is positive. As SEs are generated at the hole bottom, many will accumulate on the sides of the hole. Furthermore, a fraction of the primary electrons may backscatter (backscattered electrons—BSEs). These electrons may have energies up to the beam energy. Those with trajectories that return up the hole can easily escape the sample. However, their high energy means they escape from a range of depths at and below the hole bottom. There are relatively few BSEs to begin with (the yield is lower than the SE yield at conventional SEM landing energies), and surface information is diluted by the large fraction that originates beneath the surface. Some BSEs collide with the hole walls and generate SEs from points other than the hole bottom. These (SE_2) electrons have the same information content as the BSE from which they originate; they contribute little information about the topography of the bottom of the hole.

To combat some of the more challenging physical processes associated with imaging HAR features under conventional CD-SEM conditions, this paper explores the use of SEM and environmental SEM (ESEM) operated at a higher voltage.

If the SEM were operated at a higher voltage (around 10 keV to 15 keV), the range of the primary electrons would be greater, such that many of the primaries would penetrate through the SiO_2 layer and into the silicon substrate. A useful estimate of the electron range is the Kanaya-Okayama [7] expression, which we can write as

$$R = \alpha \frac{AE^{5/3}}{Z^{0.89}\rho} \tag{1}$$

where E is the beam energy, A and Z are the atomic weight and atomic number, ρ is the material density, and α is a constant, 5.84 x 10^{21} $kg/m^2/J^{5/3}$ in SI units (though $\alpha = 2.76 \times 10^{-10}$ $kg/m^2/eV^{5/3}$ is more convenient if E is to be given in electron volts). The range of electrons in SiO_2 is shown in Figure 4.

The large range of high energy electrons could reduce the negative charge layer from the beam electrons, present with conventional CD-SEM operating conditions, by putting most of the negative charge deeper in the sample, below the bottom of the HAR feature. However, positive charging is also reduced (fewer holes at the surface) because the SE yield (Figure 4) at energies greater than a few hundred electron volts decreases with increasing energy. Since both a desirable and an undesirable effect increase as the landing

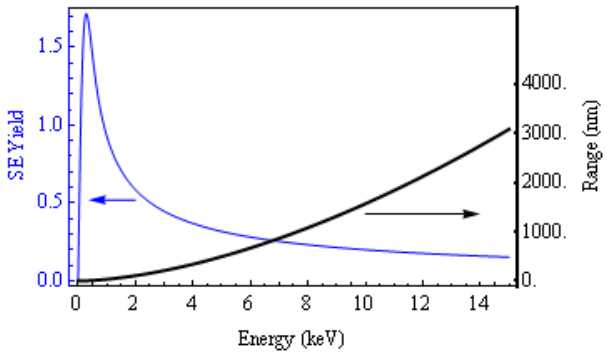

Figure 4: Range of electrons from Equation 1 (right axis) and estimated SE yield (left axis) in SiO_2.

energy increases, it is not possible except by measurement to know which effect dominates.

In ESEM imaging, the sample is imaged while in a gas atmosphere (commonly water vapor). The gas becomes positively charged in the presence of the electron beam, and the positive ions counteract the surface charge. In the specific case of imaging HAR-CTs (high aspect-ratio contacts), the ESEM helps to eliminate the buildup of negative charge in the hole. Additionally, the collision of SEs with the gas molecules ionizes the gas molecules. The ionization then generates positive ions and additional signal-carrying electrons. This cascade of events results in the amplification of the signal [8,9].

In addition to comparing results of different imaging conditions, a simulation program, JMONSEL [10,11], is used to simulate various conditions. JMONSEL follows electrons as they enter the material, lose energy, and scatter. Recent additions to JMONSEL permit it to keep track of charging in insulating parts of the tetrahedrally meshed sample. Finite element analysis periodically solves for the electrostatic potentials (and hence electric fields) associated with these charges and relevant boundary conditions (such as grounded wafer and externally imposed fields). Electron trajectories are corrected for the effects of these fields. By monitoring the electrons that exit the material and are captured, the electron yields can be found at each point and are plotted as line scans.

Simulations allow for more flexibility, both in the sample and the experimental conditions. For example, experimentally determining whether a signal received from the bottom of a hole carries information about the topography and materials can be difficult. If no contrast is detected in a measurement, is it because the measurement does not have sensitivity or because nothing is actually at the bottom of the hole to produce contrast? In a simulation, however, the program can be used to modify the structure and place topography or other materials at the hole bottoms (for example, a small copper or silicon particle).

When the goal of imaging a feature is to determine whether its bottom has been successfully imaged, determining whether the bottom is actually being seen can be difficult. If the bottoms were not successfully imaged, the image would be expected to show a bright top surface, a dark bottom surface, and presumably some transition in between. However, if the bottoms were successfully imaged, the same general appearance would be expected. Therefore, a detailed analysis of the images is necessary to determine whether or not the bottoms of the features were successfully imaged.

One method used in this work is varied tilt imaging. By imaging the sample at two angles and measuring how far the apparent bottom of the hole moves, the depth of the hole can be determined. This type of measurement requires that the microscope being used can perform tilt measurements.

When tilt mode is not available, other methods can be used. Line profiles from the image can be analyzed to see if the signal level in the hole is flat or noisy. Additionally, the gray level in the hole can be measured and compared to the zero level (obtained by blanking the beam during a portion of the image acquisition). However, even if a signal from the bottom is measured, we cannot determine if we are seeing SEs from the hole bottom (SE_1 and SE_2), SEs that were generated by a BSE at a distance from the initial impact point (SE_2), or SEs that were generated from the collision of a BSE outside the sample (SE_3). While SE_1s contain the information we are looking for, SE_2s and SE_3s carry much less information.

2. EXPERIMENTS

2.1 CD-SEM Imaging of HAR-CTs

For reference, a CD-SEM is used to image a sample set of 500 nm deep HAR-CTs. The goal is to show basic imaging

capabilities of the CD-SEM for HAR-CTs (as opposed to a systematic experiment designed to optimize the imaging to find the best conditions).

2.2 Environmental SEM and Higher Voltage SEM

To examine whether gas in the ESEM can aid the imaging of HAR-CT bottoms, the samples are imaged in a FEI Nova NanoSEM [12] using water vapor as the ambient gas and a helix type detector. To examine whether a higher voltage SEM can image the bottoms, the samples are imaged at 15 keV in a LEO 1550 SEM [12]. The detectors in both tools are on-axis.

Because the higher voltage SEM and ESEM units are not CD metrology tools, the samples must be cleaved to obtain chips small enough to fit on the stage mounts. Additionally, as opposed to CD-SEMs, these tools are unable to apply an external extraction field. This inability could decrease the capability of the tools to image the samples successfully.

2.3 JMONSEL Simulations

A variety of experiments were simulated with JMONSEL, including varying the contact hole radius and depth. Additionally, imaging a specific geometry at 500 eV and 5000 eV was compared.

3. RESULTS

3.1 CD-SEM IMAGING OF HAR-CTs

To illustrate the ability of CD-SEMs to image HAR-CTs, a sample was imaged in a Hitachi S9380 CD-SEM [12]. Images were acquired using a beam energy of 800 eV and a field of view of approximately 500 nm. As this tool is not equipped for tilt imaging, the method of analysis requires the line profiles to be examined to compare the signal levels inside and outside the holes. Figure 5 shows images of holes from the C100P200 and C60P120 arrays, as well as line profiles taken from each image.

Examining the line profile from the C100P200 scan shows that the signal from the holes is actually greater than the signal from the surface. Based on this evidence, we infer that the bottoms of this contact hole are being imaged successfully. We contrast this with the image from the C60P120 array. The line profile shows that the signal level from the holes is close to zero, hence we can state that we are unable to image the bottoms of the contact hole.

3.2 Environmental SEM and Higher Voltage SEM

Imaging with the ESEM required a careful evaluation to find the best imaging conditions. Many parameters must be optimized for the best results. The tool used had a gas pressure range of 10 Pa to 130 Pa. If the pressure used was too low, charging would distort images, if too high, excessive scattering from the beam would degrade resolution or shut down the gas phase electron cascade that serves to increase the signal. The optimal pressure in our instrument was found to be 100 Pa to 130 Pa. It was found that a minimum of 10 keV or 15 keV beam voltage was needed to obtain the sharpest quality images at the tops of the holes.

3.2.1 Measuring Depths with Varied Tilt Imaging

By taking two images at different tilts and measuring the distance that the apparent bottom moves, we can calculate the depth that we are imaging, as shown in Figure 6. The calculation is based on simple trigonometry, using the Law of Sines, as shown in equation (2) [13]. Knowing the change in the tilt angle (angle A) and the distance that the perceived bottom moves (distance a, opposite from angle A), the triangle shown in the figure can be constructed. Figure 7 shows two images taken at different tilt angles, as well as the associated line profiles. Note that the same edge is compared before and after tilting, so differences in the shape of the left and right edges do not affect the measurement. Table I shows the results from the calculation.

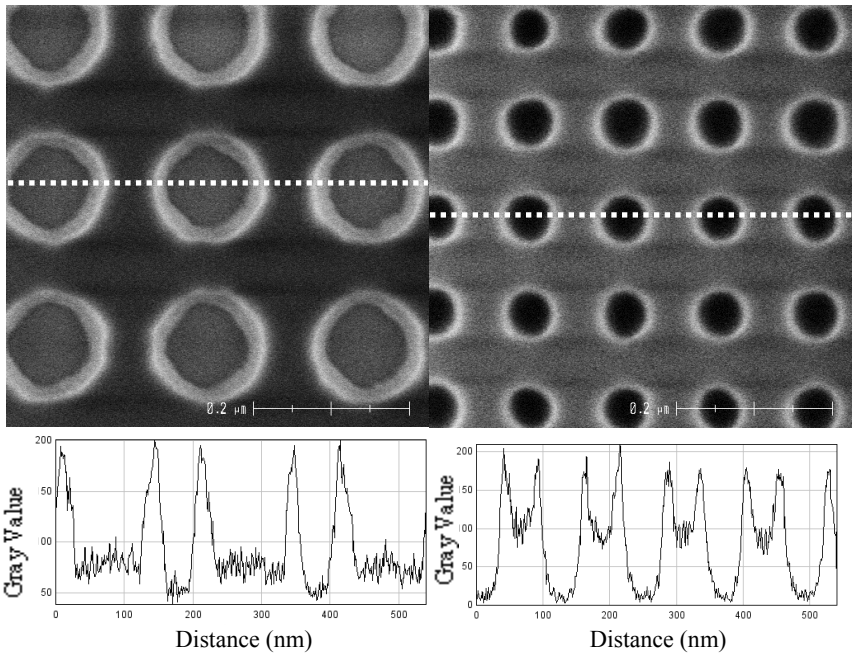

Figure 6: CD-SEM imaging of Contact Holes
Top left: Image of C100P200 array. Top right: Image of C60P120 array.
Bottom left: Line profile from top left image. Bottom right: Line profile from top right image.

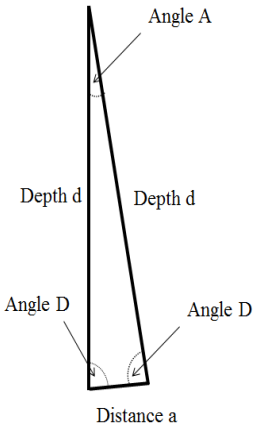

Figure 5: Schematic of tilt-measuring calculation

$$\frac{Sin(A)}{a} = \frac{Sin(D)}{d} \qquad (2)$$

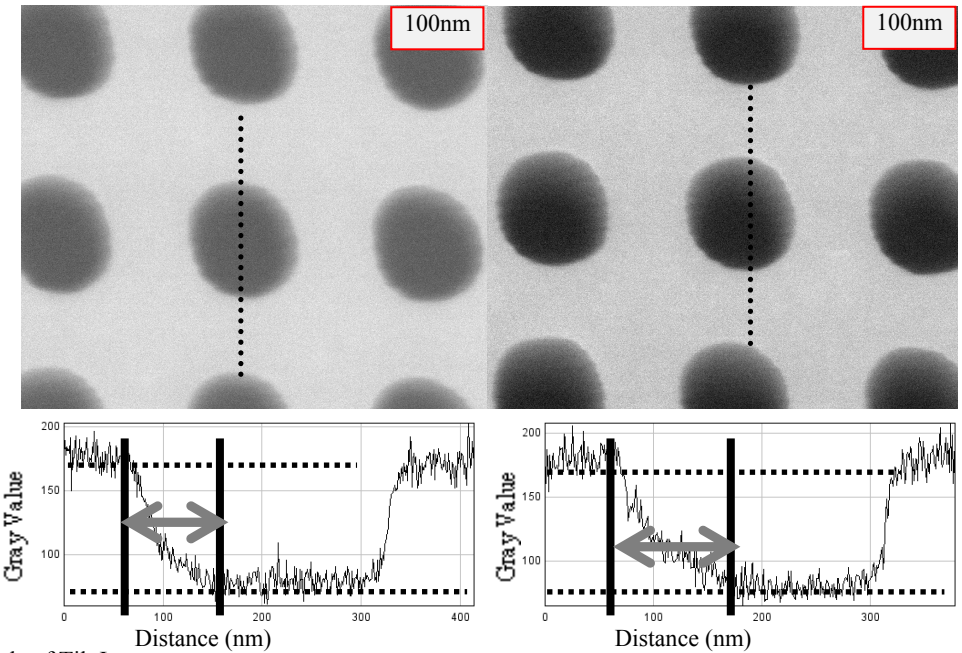

Figure 7: Example of Tilt Imaging
Top left: Image of contact holes with 0° tilt Top right: Image of contact holes at 2° tilt
Bottom left: Line profile from top left image. Bottom right: Line profile from top right image
The change in the measured distances gives us distance **a** in Figure 6.

Table I: Example Calculations for Depth Measurement

0 Degree Tilt		**2 Degree Tilt**	
Top of surface location	X = 64 pixels	Top of surface location	X = 65 pixels
Edge of hole bottom location	X = 145 pixels	Edge of hole bottom location	X = 183 pixels
Change in position (distance **a**)	37 pixels		
Change in position (distance **a**)	14.45 nm		
Measured depth (depth **d**)	415 nm		
Actual depth	1100 nm		

The overall results from the experiments with ESEM and higher voltage SEM are shown in Figure 8. According to results measuring depths by tilts, apparently we are unable to detect hole bottoms with either technique, with the tools available and conditions tried to date. But do note that this is not a final assessment, due to the following factors:

- Tools not optimized for CD measurements
- Detector improvement possible
- Pre-charge not yet attempted
- External extraction field not available (as common in CD-SEMs)

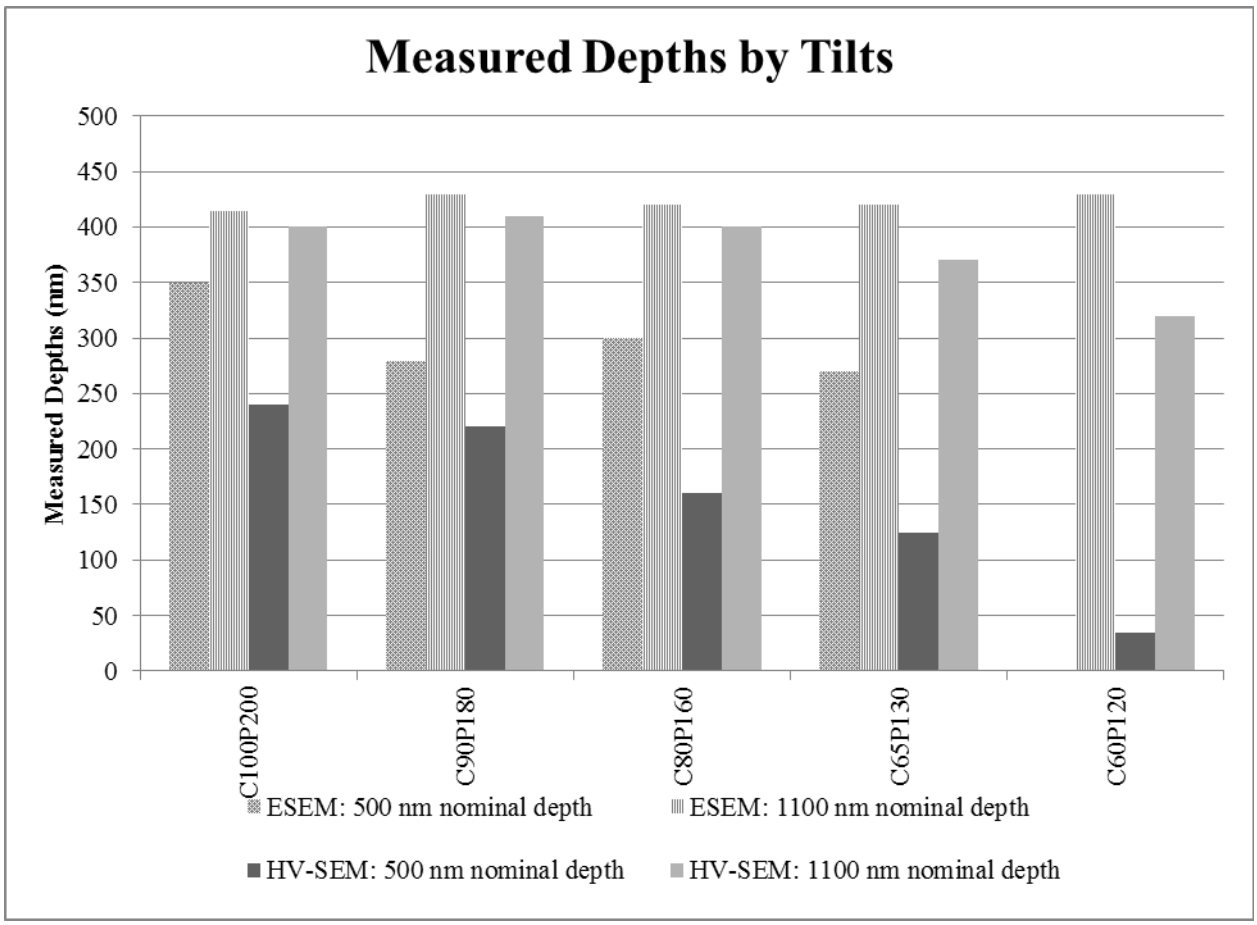

Figure 8: Measured depths by tilts. The plot shows the depths measured using the various techniques and shows that we were unable to detect the bottoms of the holes with the techniques used in the experiments.

3.3 JMONSEL Simulations

Using the JMONSEL program, several conditions were simulated, including variations in sample geometry and beam energy. Holes of different depths were simulated (500 nm, 700 nm and 900 nm), as well as holes of different widths (top/bottom radii of 70 nm/50 nm, 50 nm/35 nm and 35 nm/20 nm). One geometry was simulated with two different landing energies (500 eV and 5000 eV). As with conventional CD-SEM measurements, the goal was to understand basic physical processes at work in the reference technique rather than a systematic exploration of a large range of possible operating conditions.

Several different types of data are generated from the simulation. One is a line scan, which is a plot showing detected electron yields as a function of position (the electrons detected as the beam passes over each pixel).

One issue is the difficulty of determining whether what appears to be the bottom of a hole in the image actually is the bottom. When simulations are used, the structure can be modified. Simulations were designed that added a small cylindrical "particle" to the bottom of the hole, with a radius of 10 nm and a height of 10 nm. If the shape of the particle could be seen in the line profile, we could infer that the signal from the hole bottom can be extracted.

One set of simulations compared line profiles from scans of holes of varying widths. Two sets of geometries were used, one with a bottom particle made of copper and another with a bottom particle of silicon. Line profiles showing total yield (BSE + SE) are displayed in Figure 9. The left-right asymmetry in the regions on the top surface (outside the holes) in the simulated linescans has two causes: (1) To save memory the sample mesh was finer on the left edge than on the right. This results in finer detail (less spatial averaging) on the left than on the right. (2) Local deviations of surface potential from the average value are sensitive to small variations in local charging. These variations are due to random scattering processes. Neither of these processes significantly alters the field or imaging in our region of interest at the bottom of the hole. For the holes with the widest top radius, the bottom particle is reflected in the line scan. As the holes get progressively narrower, the signature from the particle decreases, and it can barely be seen in the narrowest holes. Additionally, detection of signal from the copper particle is much stronger than from the silicon particle. Simulations indicate that the Cu BSE yield is much higher than the Si BSE yield, which accounts for much of the difference. References likewise show that the SE yields of copper and silicon are similar at 500 eV, but that copper has a higher backscattered yield [[14]-[17]]. Therefore, based on examination of the line scans, we can infer that, although the higher energy BSEs are able to escape, it is more difficult for the lower energy SEs to escape from the bottom of the hole. For the narrowest holes, both copper and silicon particles have an extremely small signal in these low-noise simulations (5000 electrons/pixel). Under actual measurement conditions of typically 5 to 10 electrons per pixel per frame, such low signals are likely to be lost in the noise. (We will further discuss the effect of noise on detectability below.)

Another set of simulations compared line profiles from scans of holes with varying depths. Simulations were run for holes with a constant radius (top/bottom radii of 70 nm/50 nm) and depths of 500 nm, 700 nm, and 900 nm. Copper particles (defined as cylinders with a 10 nm radius and a 10 nm height) were placed at the hole bottoms, and the beam energy was held at 500 eV. Line profiles for this simulation are shown in Figure 10. The profiles indicate that the copper particle can be detected at the bottom of a 500 nm deep hole, but as the hole becomes deeper it becomes more difficult for the signal at the bottom to be detected.

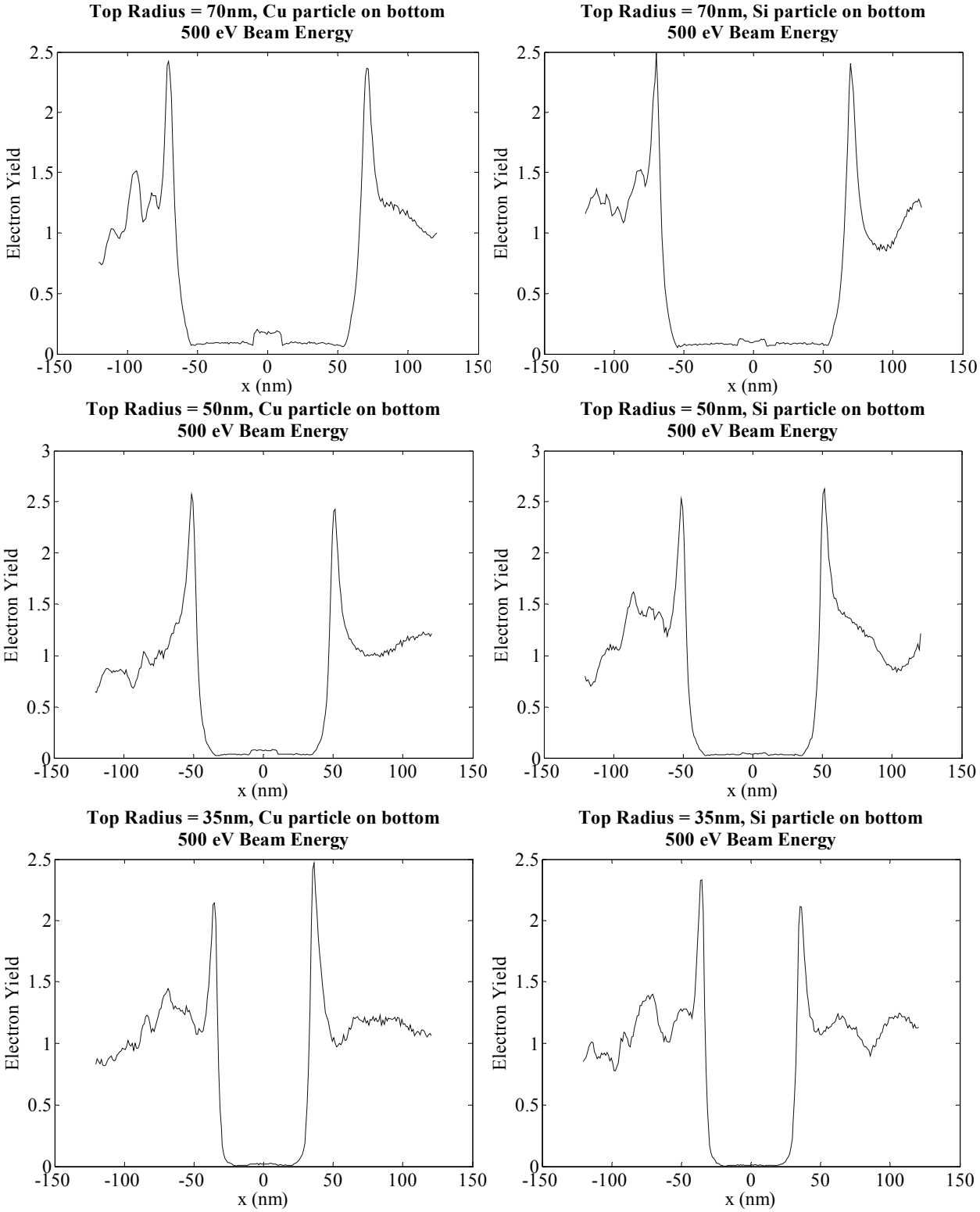

Figure 9: Simulated line profiles as a function of width, without added noise.
Top left: Top radius of 70 nm with a Cu marker particle
Top right: Top radius of 70 nm with a Si marker particle
Middle left: Top radius of 50 nm with a Cu marker particle
Middle right: Top radius of 50 nm with a Si marker particle
Bottom left: Top radius of 35 nm with a Cu marker particle
Bottom right: Top radius of 35 nm with a Si marker particle

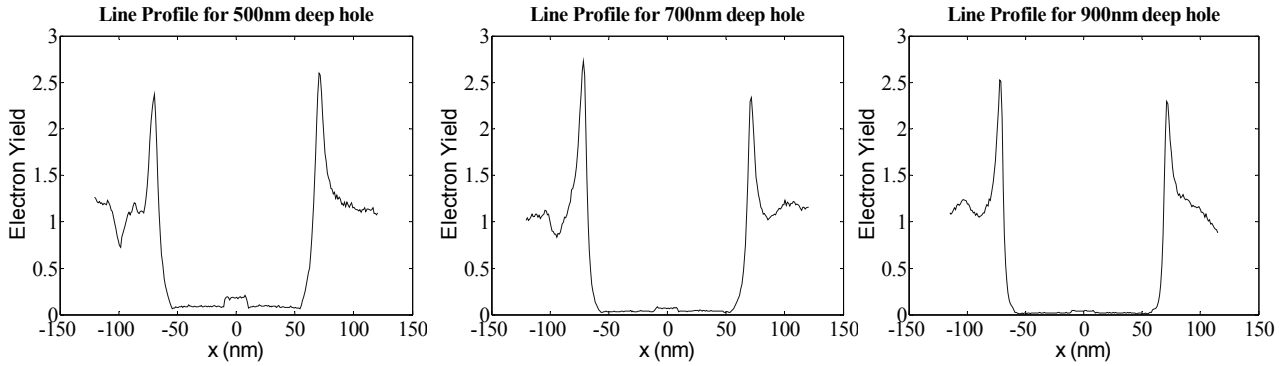

Figure 10: Simulated line profiles as function of depth, without added noise. Holes vary in depth from 500 nm (left) to 700 nm (center) to 900 nm (right)

To gain more understanding of the experimental conditions at high and low beam-energy, simulations were done to compare line scans at 500 eV (conventional CD-SEM) and 5 keV. Although the imaging experiments were done at 15 keV, for the material set in JMONSEL, using the most accurate SE generation model, the available material property data did not allow beam energies above 5 keV. The results are shown in Figure 11. When comparing the two line scans with the same sample geometry, the effect of the copper particle at the bottom of the hole is easily seen at 500 eV. However, when using 5 keV, there is only a slight perturbation in the profile near where the particle is known to be. This will make a difference to the detectability of the signal in the presence of noise, which we will discuss below.

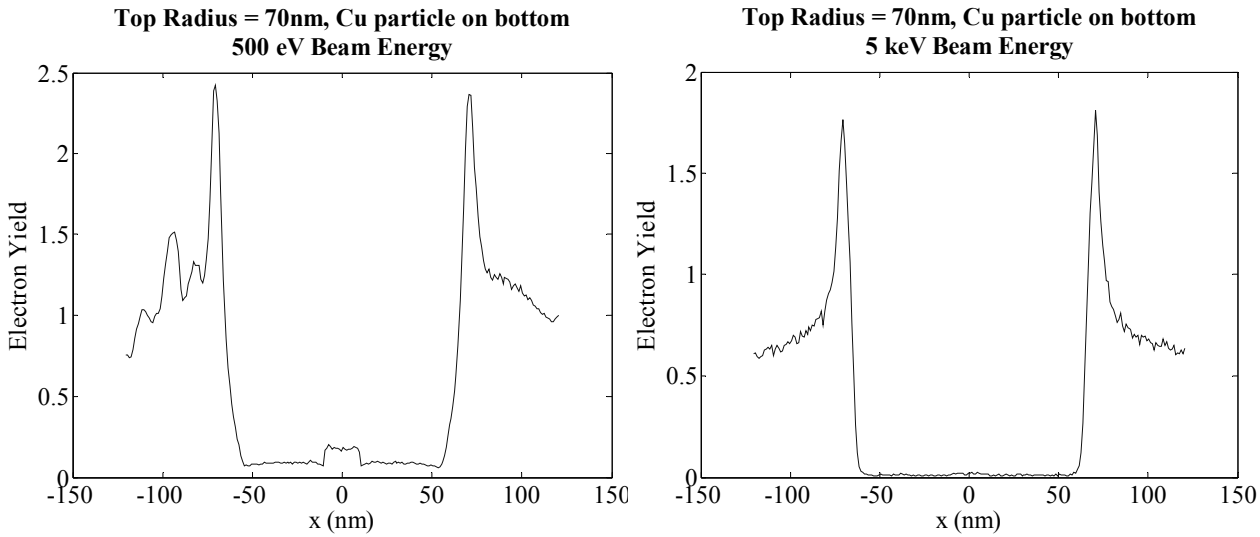

Figure 11: Simulated line profiles as a function of beam energy, without added noise.
Left: Beam energy of 500 eV with a Cu marker particle Right: Beam energy of 5 keV with a Cu marker particle

JMONSEL also allows the surface potentials to be examined. These, shown in Figure 12, explain the loss of signal with increasing beam energy. With 500 eV beam energy, the surface potential quickly saturates at a positive potential (which helps to extract SEs from the hole). With the 5 keV beam energy, the surface potential does not saturate; moreover, it is highly negative, which is counterproductive and prevents SEs from escaping the hole. The presence of any signal at all from the bottom must be due to BSEs, since only they have enough energy to overcome the charging barrier. These results illustrate what happens when the beam energy is not high enough to achieve sufficient transmission of electrons through the oxide—and therefore the hoped-for positive charging.

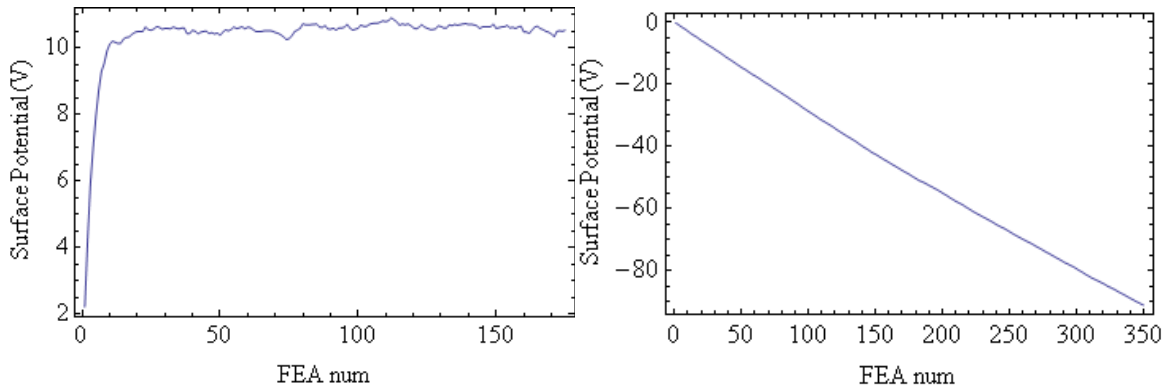

Figure 12: Surface potentials for 500 eV and 5 keV simulations vs. finite element analysis (FEA) number. The simulation performed 175 FEA per frame with 1 electron/pixel in each frame, so the left graph shows surface potential evolution during 1 frame and the right one 2 frames. Left: Surface potentials for the 500 eV simulation. Right: Surface potentials for the 5 keV simulation.

The simulated results shown thus far do not reflect any noise, which will be a part of any realistic SEM image. A quantitative way of displaying the effect of noise on the measurements is by plotting expected measurement noise and signal as a function of a parameter of interest (e.g., hole size) on the same graph. In conjunction with some criterion (e.g., signal:noise = 1), the parameter range under which a feature is detectable can be determined. For our purposes, to detect a marker particle on the bottom of a contact hole, the difference in the signal yields between the marker and the hole bottom must be greater than the noise level. The expected noise depends on the number of incident electrons per pixel (n), which is calculated according to Equation 3:

$$n = A\,\tau/e \tag{3}$$

with A the beam current, τ the total time the beam spends on a pixel (including multiple visits if the image is a multi-frame image), and e is the magnitude of the electron charge. The number of electrons per pixel will vary with imaging conditions. For our calculations, we assume a beam current of A = 10 pA and a time τ = 0.126 µs (33 ms per 512 × 512 pixel frame). With these assumptions, n is approximately 8 electrons per frame multiplied by the number of frames in the image.

If the electron yield on the marker particle is y_{mp}, the yield from the remainder of the bottom of the hole is y_b, and the number of incident electrons per pixel is n, the noise is calculated according to Equation 4.

$$\text{Noise} = 1.45\sqrt{\frac{y_{mp}+y_b}{n}} \tag{4}$$

The prefactor of 1.45 was determined by JMONSEL simulation. This factor would be 1 if the noise were strictly Poisson distributed. It is somewhat higher than 1 because the emissions of electrons are not completely uncorrelated random events. (Correlations occur, for example, when a BSE generates multiple SE_2.)

The results of the detectability calculations are shown in Figure 13. Each graph displays a signal level and corresponding noise levels for images with different numbers of frames. Graphs differ by test particle composition (Si or Cu) or by the parameter (hole radius or hole depth) on the horizontal axis. The desirable condition is for the signal curve to be above the noise curve. For a silicon particle, the signal is so weak that one would need to integrate more than 128 frames to see a signal from the widest hole. The copper particle is much easier to detect because it emits more BSEs. Figure 13

(bottom left) shows the detectability as a function of hole depth. It is shown that a 500 nm deep hole is barely detectable with 8 frame integrations.

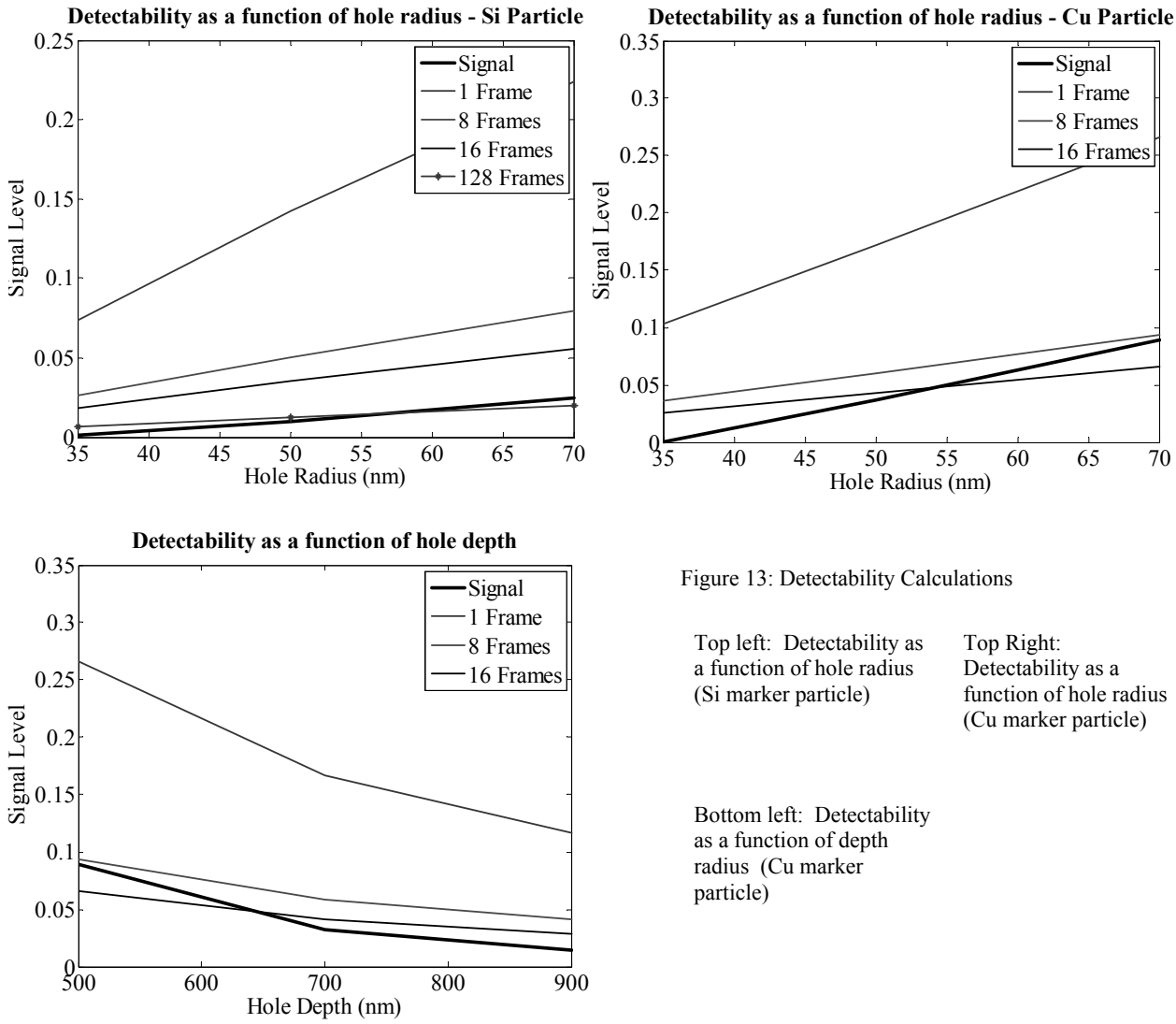

Figure 13: Detectability Calculations

Top left: Detectability as a function of hole radius (Si marker particle)

Top Right: Detectability as a function of hole radius (Cu marker particle)

Bottom left: Detectability as a function of depth radius (Cu marker particle)

This calculation can be applied to the line profiles to display the effect of noise on the scan as well. Figure 14 displays line profiles of scans from simulations of contact holes with a top radius of 70 nm and a silicon particle at the bottom of the hole. If only one frame makes up the image, the particle at the hole bottom cannot be discerned (and therefore, we can state that SEs from the hole bottom are not detected). However, if an image is acquired by integrating a substantial number of frames, we can see evidence of the particle in the linescan and hence state that SEs from the bottom are being detected.

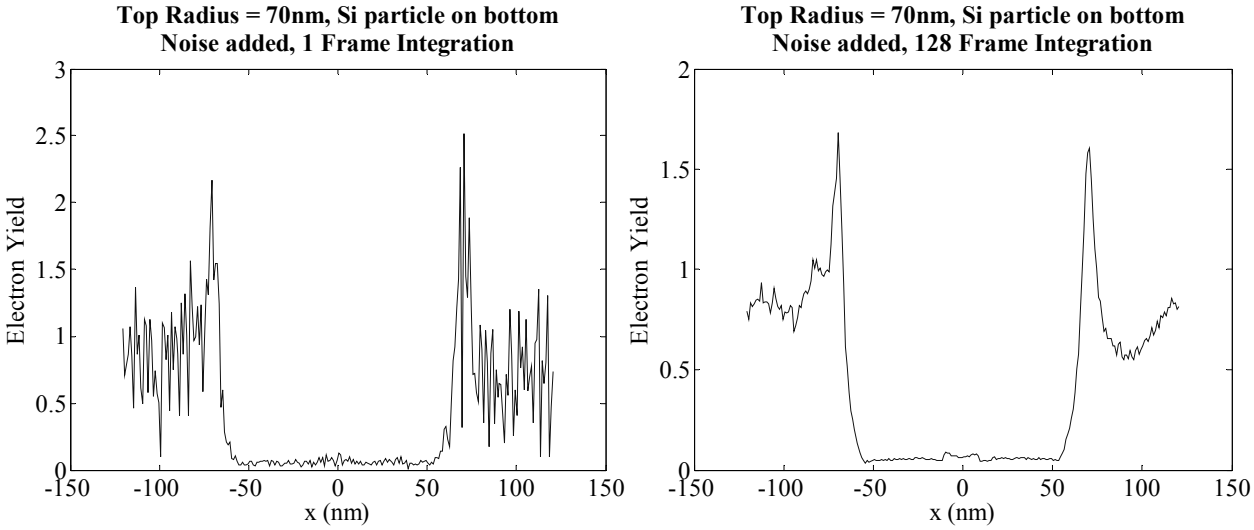

Figure 14: Line scans with different amounts of frame integrations
Left: Line scan of contact hole with only one frame integration Right: Line scan of contact hole with 128 frame integrations

4. CONCLUSIONS

Conventional CD-SEM can likely image the widest and shallowest holes from our sample set successfully. This conclusion is based on the signal level measured in the holes, as compared to the signal level on the surface outside the holes. Due to the unavailability of tilt functionality on the CD-SEM used, this could not be confirmed.

When a higher voltage or ESEM was used (in the configuration that was available during the experiments), the bottoms of the holes could not be imaged successfully. The goal of higher beam energy was to have most beam electrons transmit through the oxide, resulting in positive sample charging and a smaller dipole inside the oxide. We conclude from the measurement results and JMONSEL simulations that this goal was not achieved at the beam energies (and other measurement parameters) we tried in these measurements.

By using JMONSEL to simulate experiments, experimental conditions were found such that the signals could be detected. The SE signal from the bottom was weak under the conditions used in the simulation; consequently, many frames would need to be integrated to image the bottoms of the holes successfully. Note, however, that our conventional CD-SEM simulations did not explore the full range of operating conditions. In particular, under the conditions simulated, the oxide surface charged to only about 10 V. Our samples (with 500 nm to 1100 nm thick oxide) should be able to sustain a surface potential greater than this by a factor of 5 to 20. Higher surface potential could be achieved by using a larger extraction field to increase the charge density or by increasing the scan size to enlarge the charged area. These approaches would increase the beneficial extraction field inside the contact hole.

ACKNOWLEDGEMENTS

We thank the SEMATECH XMAG (Combined Metrology Advisory Group) and MPAG (Metrology Program Advisory Group) for their support of this project.

REFERENCES

[1] Katsumata, R. et al., "Pipe-shaped BiCS flash memory with 16 stacked layers and multi-level-cell operation for ultra high density storage devices," Symposium on VLSI Tech. Dig., pp136-137, 2009.

[2] *The International Technology Roadmap for Semiconductors* (San Jose: Semiconductor Industry Association, 2010); available from the Internet: http://public.itrs.net/.

[3] Abe, H., and Yamazaki, Y. "Error Factor in Bottom CD Measurement of Contact Hole using CD-SEM," Proc. SPIE Vol 6152, 61524H-9 (2006).

[4] Cohen-Tanugi, D. and Yao, N. "Superior imaging resolution in scanning helium-ion microscopy: A look at beam-sample interactions," J. Applied Physics, v. 104, 063504 (2008).

[5] Arceo, A., Bunday, B., Cordes, A., and Vartanian, V. "Semiconductor metrology beyond 22nm: 3D memory metrology". Solid State Technology, Feb 2012.

[6] Wang, C., Choi, K., Chen, Y. Price, J., Ho, D., Jones, R., Soles, C., Lin, E., Wu, W.L., and Bunday, B. "Nonplanar high-k dielectric thickness measurements using CD-SAXS." Proc. SPIE, v. 7272, pp 72722M (2009).

[7] Goldstein, J., and Newbury, D., et. al. *Scanning electron microscopy and x-ray microanalysis*, Springer (2003).

[8] Postek, M.E., Vladár, A.E., Bennett, M.H., Rice, T., and Knowles, R., "Photomask dimensional metrology in the scanning electron microscope, part II: High-pressure/environmental scanning electron microscope," *J. Micro/Nanolith. MEMS MOEMS*, 2, 224-231 (2004).

[9] Thiel, B.L. and Toth, M. "Secondary Electron Contrast in Low-Vacuum/Environmental Scanning Electron Microscopy of Dielectrics," J. Appl. Phys. **97**, 051101-051118 (2005).

[10] Villarrubia, J. S. , Ritchie, N. W. M., and Lowney, J. R. "Monte Carlo modeling of secondary electron imaging in three dimensions," Proc. SPIE **6518**, 65180K (2007).

[11] Villarrubia, J. S., and Ding, Z. J. "Sensitivity of SEM width measurements to model assumptions," J. Micro/Nanolith. MEMS MOEMS **8**, 033003 (2009)

[12] Commercial equipment is identified in this report in order to describe the experimental procedure adequately. Such identification does not imply recommendation or endorsement by the National Institute of Standards and Technology, nor does it imply that the equipment identified is necessarily the best available for the purpose.

[13] Swokowski, E., and Cole, J., *Algebra and trigonometry with analytic geometry*, Cengage Learning (2007).

[14] Dione, G.F., "Effects of secondary electron scattering on secondary emission yield curves," J. Appl. Phys., 44, 5361-5364 (1973).

[15] Dione, G.F., "Origin of secondary-electron-emission yield-curve parameters," J. Appl. Phys., 46, 3347-3351 (1975).

[16] Shimizu, R., "Secondary electron yield with primary electron beam of kilo-electron-volts," J. Appl. Phys., 45, 2107-2111 (1974).

[17] Koshikawa, T., and Shimizu, R., "Secondary electron and backscattering measurements for polycrystalline copper with a spherical retarding-field analyzer," J. Phys. D., Appl. Phys., 1369-1380 (1973).

SPIE paper # 8324-56